Article | Received 26 July 2025; Revised 4 October 2025; Accepted 5 October 2025; Published 8 December 2025
https://doi.org/10.55092/aimat20250015

Supplementary material

Multi-scale modelling of mechanical responses of FeCrAl alloys with solid-solution and processing effects

Zhen Liu[1,2,†], Yaolin Guo[3,†], Jingyu Zhang[4,5,†], Yifan Li[2], Zheyu Hu[6], Muhammad Adnan[3,7], Nianxiang Qiu[8], Shurong Ding[5,*] and Shiyu Du[2,3,6,*]

[1] Ningbo Key Laboratory of High Performance Petroleum Resin Preparation Engineering and Technology, Ningbo Polytechnic University, Ningbo 315800, China
[2] College of Materials Science and Chemical Engineering, Harbin Engineering University, Harbin 150001, China
[3] Ningbo Institute of Materials Technology & Engineering, Chinese Academy of Sciences, Ningbo 315201, China
[4] State Key Laboratory for Turbulence and Complex Systems, Department of Mechanics and Engineering Science, BIC-ESAT, College of Engineering, Peking University, Beijing 100871, China
[5] Institute of Mechanics and Computational Engineering, Department of Aeronautics and Astronautics, Fudan University, Shanghai 200433, China
[6] School of Materials Science and Engineering, China University of Petroleum (East China), Qingdao 266580, China
[7] University of Chinese Academy of Sciences, Beijing 100049, China
[8] Yangtze Delta Region Institute (Huzhou), University of Electronic Science and Technology, Huzhou 313001, China

† These authors contributed equally to this work.

* Correspondence authors; E-mails: dingshurong@fudan.edu.cn (S.D.); 20220133@upc.edu.cn (S.D.).

S1. Fitting procedure of elastic constants for FeCrAl alloys

The elastic properties are not the main focus, but serve as the basis in the multiscale model. In fact, elastic modulus data for similar alloys have been measured experimentally, including Young's modulus E, shear modulus G and Poisson ratio ν, at different temperatures [1]. The shear modulus ($\mu(c,T)$) of isotropic material can be obtained accordingly. In this study, $\frac{\mu(c,T)}{\mu(c,0)}$ in Equations (7) and (9) is fitted for the experiment data of C35M3 alloy as

$$\frac{\mu(c,T)}{\mu(c,0)} = \left(1 - \left(\frac{T}{1800}\right)^2\right) \tag{S1}$$

where, $\mu(c,0)$ is the shear modulus at 0 K and T is temperature in K.

However, the elastic constants C_{11}, C_{12} and C_{44} of single crystals can not be directly determined from E and ν. On the other hand, atomic methods are often used to estimate the macroscopic equivalent elastic modulus by some approximate method, like Voigt-Reuss-Hill (VRH) model. However, it is still difficult to obtain the elastic constants consistent with experimental data in the whole temperature range by DFT or MD simulations. If it is assumed that the relationship between single crystal elastic constant and macroscopic elastic modulus can be completely described by the VRH model, from a practical point of view, one can derive a set of corresponding elastic constant formulas from experimental data with some additional conditions.

Simmons *et al.* [2] reported that Al content effect on C_{44} ($(dC_{44}/dc_{Al})_{RT}^{\exp} = 0.39$ GPa/at%) is much lower than that on C_{11} and C_{12}. Therefore, it is reasonable to assume that $dC_{44}/dc_{Cr} = dC_{44}/dc_{Al} = 0.39\ GPa/at\%$. In pure iron, the variation of C_{11} with temperature is found to be very similar with that of E. Then, it is presumed that $C_{11}(T) = k_{el}E(T)$ for FeCrAl alloys, where k_{el} is the conversion constant. Now, ignoring the influence of trace elements such as Mo and Si, the single crystal elastic constants of FeCrAl alloy are calculated through the following procedures (1)–(3):

(1) $C_{44}(T_{room})$ for pure iron is 115 MPa. Combining the approximation of $(dC_{44}/dc_{Al})_{RT}^{\exp} = 0.39$ GPa/at%, the C_{44} for C35M alloy with component Fe-13.2Cr-9.8Al at% can be calculated as 124.4 GPa.

(2) Based on the result of $C_{44}(T_{room})$, $C_{11}(T_{room})$ and $C_{12}(T_{room})$ can be uniquely derived from the experimental measured $E(T_{room})$ and $\nu(T_{room})$ via the VRH model. Thus, $C_{11}(T_{room})$ is found to be 197.15 GPa with $k_{el} = E(T_{room})/C_{11}(T_{room}) = 1.04$.

(3) After having the approximate formula of $C_{11}(T)$ in the full temperature range, $C_{12}(T)$ and $C_{44}(T)$ can be obtained via the VRH model with the experimental measured $E(T)$ and $\nu(T)$.

As a result, $C_{ij}(T)$ for Fe-13.2Cr-9.8Al alloy is fitted with quadratic polynomial formula as:

$$\begin{aligned} C_{11}(T) &= 2.05\times10^{2} - 8.64\times10^{-3}T - 5.44\times10^{-5}T^{2} \\ C_{12}(T) &= 121\times10^{2} + 2.98\times10^{-3}T - 3.75\times10^{-5}T^{2} \\ C_{44}(T) &= 133\times10^{2} - 2.35\times10^{-2}T - 2.62\times10^{-5}T^{2} \end{aligned} \tag{S2}$$

S2. The details of molecular dynamics model

S2.1. Solute-dislocation interaction energies

For the screw dislocation structures, the EAM potential from Mendelev [3] is chosen and the kink pair structure 1/2<111> of screw dislocation is constructed by connecting the easy-core and Mpoint core to form the Easy-Mpoint-Easy structure. The atomic structure size of the screw kink model is $300\times100\times100$ Å. For the solute-dislocation interaction energy $U_{dis}^{X}(\mathbf{r})$, the available Mendelev-based potentials from FeCr, FeAl are applied. The $U_{dis}^{X}(\mathbf{r})$ calculation range is within the cylindrical zone with radius 8 Å near the screw core along the dislocation line.

For edge dislocations, the MEAM potential from Lee [3] is selected for the VMA model parameters and edge dislocation structure relaxation. The atomic volume Ω_0 and the bulk modulus K are calculated in $10\times10\times10$ super cells at 0 K. The Voronoi method is used for atomic volume calculation and the VRH model is applied for bulk modulus calculation. Atomic volume evolutions with solute contents

curves are calculated in the 20 × 20 × 20 super cells with random substitution defects with content range 0–6 at% to estimate the size misfit parameters ε_α^X as $\varepsilon_a^X = 1/3\varepsilon_V^X = 1/3\left(1/V_0 \times dV/dc_X\right)_{c=0}$. For edge dislocation core structure, the 1/2<111>110 edge dislocation is constructed with size 80 × 80 × 80 Å. The substitution-edge interaction energies $U_{dis}^X(\mathbf{r})$ for Cr, Al are calculated with the FeCr, FeAl-MEAM potentials [3]. In Figure 4b, since the value of Γ_e has no influence on w_e^{crit} selection, Γ_e is simplified taken as 1eV/Å and the $\Delta\tilde{E}_{tot}(w_e)$ curve for Fe-Cr system are multiplied by 4 to reduce the magnitude gap with Fe-Al curves.

S2.2. Microscale fracture energy

According to Equation (14), $G_{i0}(c)$ is an idealized parameter, which represents the fracture energy for random solute single crystal near 0 K and is expected to be evaluated by MD method. For FeCrAl alloys, a series of single crystal with different tensile directions are constructed with the model size of 100 × 100 × 120 Å (Z axis is the tensile direction), and the composition is Fe-13Cr-5Al wt% (Fe-13.2Cr-9.8Al at%). The FeCrAl EAM ternary potential from Liao [3] is adopted and the tensile simulations are organized with the tensile strain 1×10^8/s at 20 K. The stress-strain (SS) curves are recorded during the tensile simulations and the microscopic effective plastic work G_{i0} is calculated as

$$G_{i0} = \int_{\varepsilon<\varepsilon_{break}} \tau d\varepsilon \tag{S3}$$

where ε_{break} is the fracture strain and determined as the sudden drop of stress. Since the anisotropy of single crystal has great influence on the deformation behaviors, the shape of the stress-strain (SS) curves with the tensile directions of <11x> ($x \in \{0, 1/2, 1, 3, 4, 6, 8\}$) and <001> are compared to analyze the deformation mechanisms, as shown in Figure S1a.

When $x \leq 1$, the fracture happens after the elastic deformation region and the plastic deformation is not obvious. On the other hand, when $x \geq 3$ the obvious plateaus appear in the SS curves and the ε_{break} of the plastic deformation plateaus increase with x, so as G_{i0}. For these cases, the microscopic plastic deformation mechanism for BCC iron is the crystal rotation accompanied by local phase transformation. More specifically, the close-packed $\{110\}$ plane rotates to the tensile direction and the BCC $\{110\}$ plane changes to the FCC$\{111\}$ plane, as shown in Figure S1b. The solute atoms hinder the formation of stable FCC phase instead by the irregular phase. Compared with FCC phase, the irregular phases have poor stress release ability, which leads to local stress concentration and fracture advance. Figure S1c shows the evolution of G_{i0} and maximum transformational FCC phase ratio P_{FCC} with solute composition for Fe-xCr-xAl (at%) alloy. G_{i0} decreases rapidly with low content and then keeps plateau, which shows that the plastic deformation behavior is not sensitive to the composition at high content. This trend is consistent with the phenomenon observed in the experiment. Therefore, the solute effects on microscopic fracture energy are comparable to the macroscopic mechanism. As a result, $G_{i0}(c)$ with component Fe-13.2Cr-9.8Al is calculated as the average value with tensile directions from $\langle 113 \rangle$ to $\langle 118 \rangle$. The result is 16.5×10^8 J/m^3, which is just in the same magnitude with the fitting parameter G_c ($2.3 - 6.8 \times 10^8$ J/m^3) from CPFEM at room temperature.

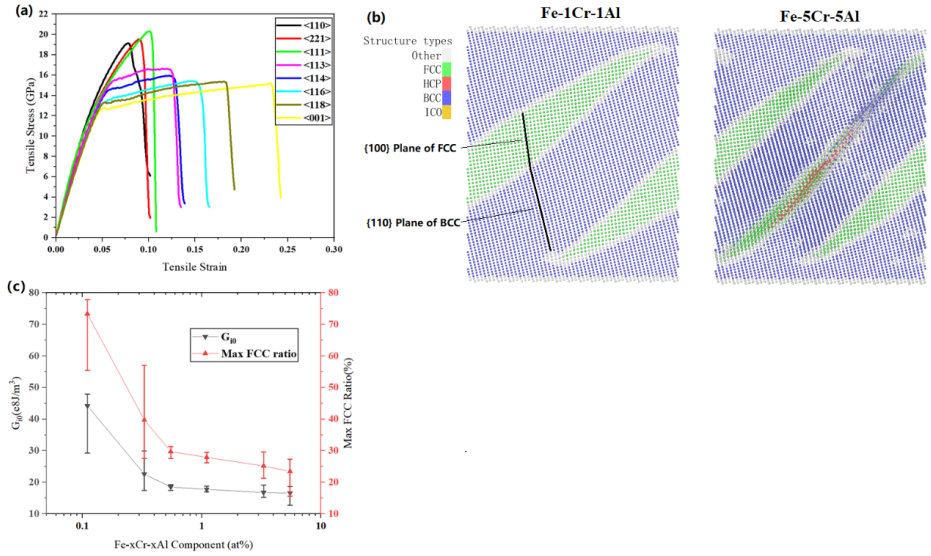

Figure S1. Results of tensile simulation from MD. **(a)** The stress-strain curves for Fe-13.2Cr-9.8Al (at%) single crystal with different tensile directions at 20 K; **(b)** The atomic structure of Fe-1Cr-1Al and Fe-5Cr-5Al (at%) alloys with 10% applied strain with <116> tensile direction. The color stands for the atomic structure type from the common neighbor analysis (CNA); **(c)** The average plastic work and maximum FCC phase ratio affected by the component for Fe-xCr-xAl (at%) alloy.

S2.3. Grain boundary energy

For grain boundary energy γ_{GB}, a series of symmetric tilt grain boundary (STGB) models with the <110> rotation axis and small Σ-value boundary planes including {331}, {552}, {221}, {332}, {554}, {111}, {556}, {335}, {112}, {113}, {114}, {115} and {118} are created. The formula for γ_{GB} calculation is as follows

$$\gamma_{GB} = \frac{E_{tot} - E_{ref1} - E_{ref2}}{2A} \tag{S4}$$

where E_{tot} is the total energy for the grain boundary system, E_{ref1} and E_{ref2} is total energy of the constituent single crystals, A is the grain boundary area. The atomic structure size of STGB models is 200 × 200 × 100 Å, the area of GB plane are quadrupled to reduce the effects of solute randomness. The FeCrAl EAM potential from Liao [3] is adopted for MD calculation. The γ_{GB} calculation are repeated 5 times with different random solute initial structures. Figure S2 shows the results of γ_{gb} at different temperature. The temperature dependent γ_{GB} are fitted via the quadratic polynomial function as

$$\gamma_{GB}(T) = 1.37[1 - (\frac{T}{1800})^{0.73}]^{0.36} \tag{S5}$$

where 1.37 J/m^2 is the average grain boundary energy at 0 K and 1800 K is the melting temperature of FeCrAl alloy. The predicted γ_{GB} at 873 K and 1073 K are 0.99 and 0.9 J/m^2 respectively, close to the typical value 1 J/m^2 for pure Fe, which indicates the reliability of the γ_{GB} calculation model.

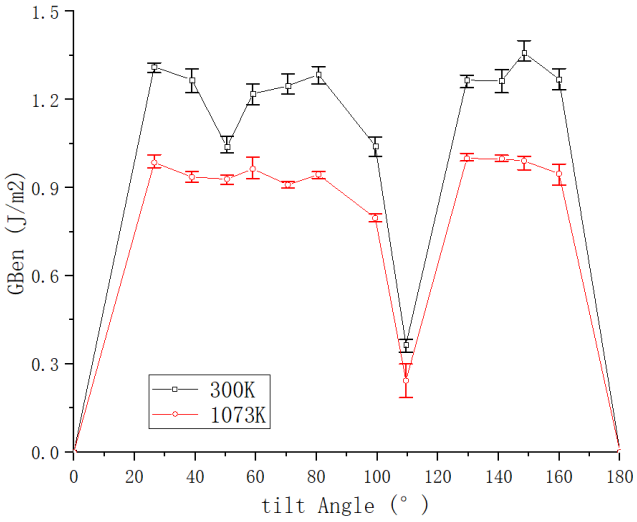

Figure S2. The grain boundary energy calculation results for Fe-13.2Cr-9.8Al alloy with different tilt angle and temperature.

References

[1] Thompson ZT, Terrani A Kurt, Yamamoto Y. Elastic Modulus Measurement of ORNL ATF FeCrAl Alloys. 2015. Available: https://info.ornl.gov/sites/publications/files/Pub59679.pdf (accessed on 20 July 2025).

[2] Simmons G, Wang H. Single crystal elastic constants and calculated aggregate properties. *J. Grad. Res. Cent.* 1971, 34(1):1.

[3] Liao X, Gong H, Chen Y, Liu G, Liu T, *et al.* Interatomic potentials and defect properties of Fe–Cr–Al alloys. *J. Nucl. Mater.* 2020, 541:152421.